UCLA
UCLA Previously Published Works

Title

What does graphitic carbon nitride really look like?

Permalink

Journal

ISSN

Authors

Melissen, Sigismund TAG
Le Bahers, Tangui
Sautet, Philippe
et al.

Publication Date

DOI

Supplemental Material

Peer reviewed

PCCP

What Does Graphitic Carbon Nitride Really Look Like?[†]

Sigismund T.A.G. Melissen,[a] Tangui Le Bahers,[b] Philippe Sautet,[c,d] and Stephan N. Steinmann,[*b]

Graphitic Carbon Nitrides (g-CNs) have become popular light absorbers in photocatalytic water splitting cells. Early theoretical work on these structures focused on fully polymerized g-C_3N_4. Experimentally, it is known that the typically employed melamine polycondensation does not go toward completion, yielding structures with ∼15 at.% hydrogen. Here, we study the conformational stability of "melon", with the $[C_6N_9H_3]_n$ structural formula using DFT. Referencing to a 2D melon sheet, B3LYP-dDsC and PBE-MBD computations revealed the same qualitative trend in stability of the 3D structures, with several of them within 5 kJ/mol per tecton. Fina's orthorhombic melon is the most stable of the studied conformers, with Lotsch' monoclinic melon taking an intermediate value. Invoking a simple Wannier-Mott-type approach, Fina's and Lotsch' structures exhibited the lowest optical gaps (2.8 eV), within the error margin of the experimental value (2.7 eV). All conformers yielded gaps below that of the monolayer's (3.2 eV), suggesting Jelley-type ("J") aggregation effects.
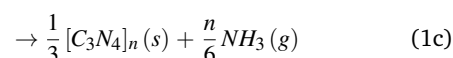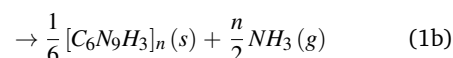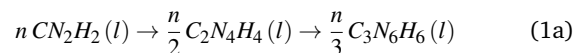
1 Introduction

As an alternative to photovoltaics, solar energy can be stored in the form of chemical bonds, counteracting the diurnal variation in solar power. To design chemical schemes allowing such storage, inspiration can be drawn from the photosynthetic process found in nature. Such schemes are commonly referred to as "artificial photosynthesis".[1]

An elegant route to perform artificial photosynthesis is by using graphitic (g-) carbon nitride (CN), with general formula g-$C_xN_yH_z$, as photoharvester[2–8] in photocatalytic water splitting cells.[9,10] Its synthesis from basic petrochemicals is cheap and straightforward, while allowing a wide structural variety.[11] Furthermore, putting such compounds to use in renewable energy sources, instead of in fuels, is environmentally beneficial.[12]

In Eq. 1 the formal reaction scheme from cyanamide to g-C_3N_4 is

provided.[13]

$$n\,CN_2H_2\,(l) \rightarrow \frac{n}{2}\,C_2N_4H_4\,(l) \rightarrow \frac{n}{3}\,C_3N_6H_6\,(l) \quad (1a)$$

$$\rightarrow \frac{1}{6}\,[C_6N_9H_3]_n\,(s) + \frac{n}{2}\,NH_3\,(g) \quad (1b)$$

$$\rightarrow \frac{1}{3}\,[C_3N_4]_n\,(s) + \frac{n}{6}\,NH_3\,(g) \quad (1c)$$

In Fig. 1 the key species discussed in this study are depicted. The melamine core can be integrated directly as a tecton yielding gt-CNs (t for triazine). The melem core, however, yields the more stable gh-CNs (h for heptazine).

Following pioneering theoretical work by Liu and Prewitt in the late 1980s,[14,15] many computational studies have been devoted to fully deaminated CN. gt-C_3N_4,[16] gh-C_3N_4,[17–19] and other polymorphs[20,21] have been extensively studied, even though it is well known that these species are unstable,[22] decomposing at the synthesis temperature that would typically be required to produce them.[23] Furthermore, frequent presentation of these fully deaminated structures as flat,[18,24] rather than corrugated,[3,25] added further confusion to the research field. Finally, the community investigating the photocatalytic activity of these structures doubts that by increasing the degree of polycondensation, increasing photocatalytic activity should always be found: participation of N lone pairs in denser π-aromatic networks reduces their ability to bond to the noble metal cocatalyst that enables the half reaction leading to H_2, and defects - rather than always trapping electrons or holes - possibly enhance the reaction.[7,26–34] We re-

[a] Université de Lyon, Université Claude Bernard Lyon 1, CNRS, Institut Lumière Matière, F-69622 Lyon, France

[b] Université de Lyon, Université Claude Bernard Lyon 1, Ecole Normale Supérieure de Lyon, CNRS, 46 allée d'Italie, F-69007 Lyon Cedex. E-mail: stephan.steinmann@ens-lyon.fr

[c] Department of Chemical and Biomolecular engineering, University of California, Los Angeles, Los Angeles, CA 90095, USA

[d] Department of Chemistry and Biochemistry, University of California, Los Angeles, Los Angeles, CA 90095, USA
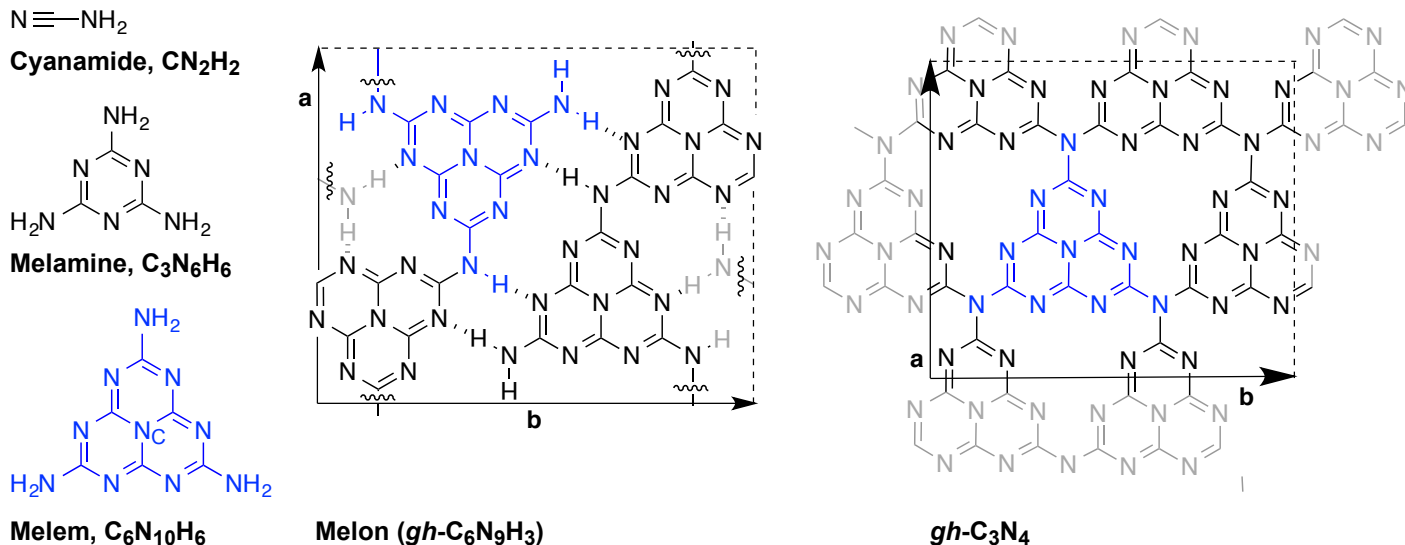
Fig. 1 Overview of structures involved in the CN synthesis process. Melem's core N atom is indexed C.

ported earlier[22] that among the different polymeric species that form during CN synthesis, gh-$C_6N_9H_3$,[35] known as "melon" is the most stable one.

Melon can be synthesized using starting materials comprising a wider range of chemical elements than C, N and H alone, such as urea $(CO(NH_2)_2)$[36] and thiourea $(CS(NH_2)_2)$.[37] Lotsch and co-workers[23,28,35] established the synthesis temperature range for the typical melamine precursor. Polymerization onset[28,38] occurs at 380 °C (in an open vessel). At the high end of this range crystalline[35] melon is produced (630 °C, closed vessel conditions). At higher temperatures the onset of material degradation is observed.[23,38] In practice, the experimental parameters are often compromises between these extremes.[38–40]

The stability of g-CN is largely due to the specific balance between steric repulsion, hydrogen bonding and the formation of a π-conjugated network. As can be understood from Fig. 1, the lone pairs in the hypothetical gh-C_3N_4 repel each other forcing a (partial) breaking of the overall π-conjugation, and causing the material to be corrugated. The hydrogen atoms in gh-$C_6N_9H_3$ stabilize several of these lone pairs, spatially separate others, and allow the formation of a flat, aromatic network overall.[22] The flat laminae themselves are interesting and can be integrated into other structures. Indeed, the Van der Waals structures they can form are not just those that are created by stacking with itself, but also by interleaving other species.[41] Within this strategy, interleaving with molybdenum dichalcogenides to allow fast charge separation is of particular experimental[42] and theoretical interest[43]. Here, we focus on the question what particular lamination pattern between gh-$C_6N_9H_3$ layers yields the most stable form of melon.

In 2015, Fina et al.[40] published a neutron-scattering study of a melon conformer with a different packing structure from the one determined by Lotsch et al. in 2007.[35] Both Fina and Lotsch synthesized the conformers studied here from melamine in a sealed environment, the main differences in protocol being the temperature, 500 °C in Fina's case and 630°C in Lotsch' and working in a

sealed ampoule (Fina) or under ammonia (Lotsch). The influence of the synthesis conditions on the obtained polymorph and the significant impact that it can have on photoactivity, has been described before for other organic semiconductors.[44] Furthermore, the structure analysis temperature could also affect the particular crystal structure observed.[45]

In Fig. 2, the possible variations in stacking patterns studied here are provided. Essentially (Fig. 2a), the shaded layer below the reference layer can shift in the hydrogen bonding direction (corresponding to **b**) by d_H, and/or in the covalent bonding direction by d_{Cov}. Second (Fig. 2b,c), the stacking pattern can be ABAB, or AAAA. In the latter case, AA-stacking does not mean that the layers are sandwich stacked. Rather, π-aromatic systems such as those discussed here tend to shift slightly with respect to each other.[46] Finally, variations in interaromatic distances (d_{Ar-Ar}), as well as in the lattice vectors within the aromatic plane are possible (arbitrarily referred to here as **a**, **b**), although these variations are typically smaller.

We study four important conformers reported in the literature. The first conformer is named "Lotsch", representing the first melon characterized. It has an AA stacking pattern and $d_H = 0$. The structure determined from the aforementioned neutron scattering study is named "Fina", with $d_H \neq d_{Cov} \neq 0$ and AB-stacking. The third and fourth structures are included in Fina's comparison and here the same labels are adopted, namely S1 for the alternative monoclinic structure and S2 for the alternative triclinic structure. S1 has an AA stacking pattern and $d_{Cov} = 0$. For S2, like Fina, $d_H \neq d_{Cov} \neq 0$, but the stacking pattern is AA. Included in the comparison are lastly 1D and 2D melon.[22]

A 2010 study[47] that combined combined theory (molecular mechanics level of theory[48]) and dedicated Nuclear Magnetic Resonance (NMR) experiments[49] of melon conformers suggested that configurations resembling Lotsch' – with $d_{Cov} = 0$ – and Fina's – with $d_H \gg d_{Cov} > 0$ – to be the two prevalent ones within melon macrostructures. These authors further proposed that the proximity in energies of the structures was the reason that ex-
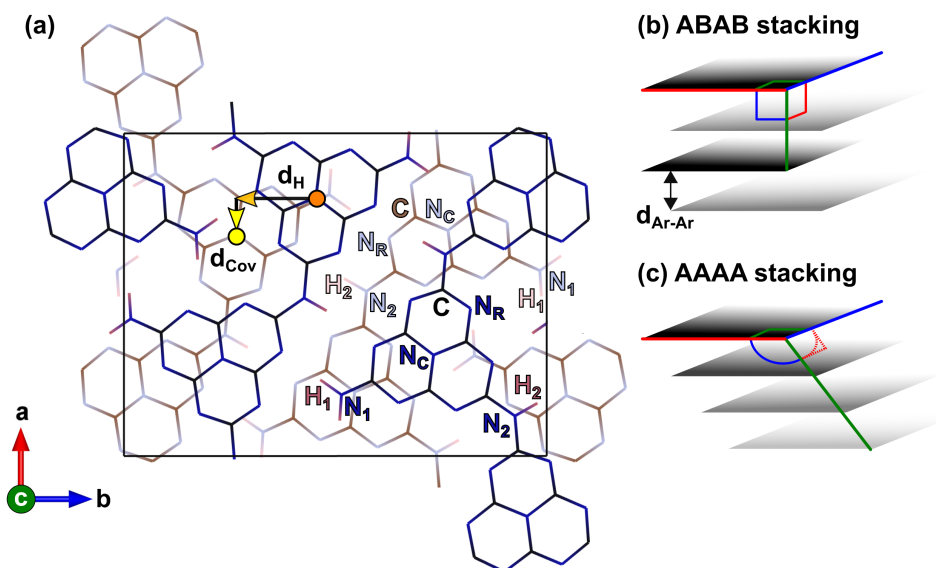
Fig. 2 Crystallography of melon. (a) Representation of an arbitrary melon bilayer. Black and brown: C; blue shades: N; pink shades: H. To guide the eye, chemically different atoms are marked, in particular the ring (R), core (C) nitrogen atoms and the primary (1) and secondary (2) amine groups are highlighted for a top and bottom heptazine subunit of choice. d_{Cov} is the distance the lower layer moves along the "covalent bonding direction" (a-direction) with respect to the top layer. d_H is the distance the lower layer moves along the "H-bonding direction" (b-direction) with respect to the top layer. Distances in the opposite direction of this choice of unit cell, are written with a minus sign. The distances are taken from N_C to the nearest next N_C (see Fig. 1). (b) One organizational form of the melon layers is by A-B-A-B stacking, leading to an orthorhombic structure. The distance between two layers is systematically referred to as d_{Ar-Ar}. (c) Alternatively, the layers organize following a systematic shift in the same direction, leading to a monoclinic or trigonal lattice.

perimentally, no definitive ordering for the stacking direction is found, and indeed a random combination of the above stacking types is likely.

We herein revisit the most important proposals for a crystalline structure of melon polymorphs by using state of the art hybrid density functional theory (DFT) computations to differentiate the stability of the various melon conformers. Given the increasing use of the *g*-CN family of compounds for a variety of purposes,[50] such a comparative work using first principles approaches is timely.

2 Computational Details

Following our earlier work,[22] DFT computations were performed using B3LYP,[51–53] which was proven earlier to yield accurate thermochemistry for *g*-CNs.

Geometry optimizations (freezing only the space group symmetry, thus leaving the cell constants fully, and the Wyckoff positions partially, free) and frequency computations - invoking the harmonic approximation - were performed with the CRYSTAL14 suite[54,55] starting from the geometries as they were provided in Lotsch' and Fina's original papers. Gatti's[56] all-electron 6-31G(d,p) basis set[57] was used for these calculations. The fundamental gaps were determined through subsequent single point calculations with the triple-ζ basis set by Peintinger *et al.*[58]. The optical gaps were then determined by invoking a simple Wannier-Mott model.[59] Its combination with hybrid-DFT was described earlier by us,[60] and it has proved to yield good correspondence to experiment.[5,61,61–66]

Civalleri's "D*" variation[67,68] to the semi-empirical Grimme D2

framework[69] was used to describe dispersive interactions, with the scaling factor s_6 equal to 0.35. This scaling factor avoids the underestimation of non-covalent bond lengths often found in molecular crystals when using Civalleri's default scaling factor of 1.0. For these calculations, the electronic convergence criterion was set to 10^{-10} Ha.[70]

The electronic energies were determined on the optimized structures using the projector augmented-wave (PAW) formalism to account for the ion-electron intraction[71] as implemented in VASP 5.4.1,[72–75] with "hard" pseudopotentials datemarked 06Feb2004. The wave function was expanded in a plane wave basis set, characterized by a cut-off energy of 600 eV. The use of plane waves has the additional benefit of being intrinsically free from the basis set superposition error (BSSE).[76,77] Dispersion interactions were refined by using the dDsC[78] and Grimme's D3 formalism with Becke-Johnson damping (D3BJ)[79] dispersion corrections. For comparison, Perdew-Burke-Ernzerhof exchange and correlation functional (PBE)[80,81] computations with both many body dispersion (MBD)[82–84] and dDsC[78] (see Table S2 in the ESI†) long range corrections were performed. Vacuum layers of >15 Å were used to suppress spurious interactions for the 1D and 2D melon. An electronic convergence criterion of 10^{-6} eV was imposed. Gaussian smearing with $\sigma = 0.01$ eV was employed.

Because of the different basis sets and associated computational cost for the two codes, the K-point samplings[85] for the VASP calculations were different from those using CRYSTAL14 (*cf.* Table 1).[86] However, convergence tests at the PBE level of theory have shown the relative energies to be converged within 1 kJ/mol per tecton with the chosen setup in VASP. The optimized structures'

Table 1 K-point Meshes used for the Brillouin Zone Integration

Species	C14 grid	VASP grid
Fina	$4 \times 4 \times 4$	$2 \times 2 \times 2$
P2$_1$/a	$4 \times 4 \times 4$	$2 \times 2 \times 2$
S1	$4 \times 4 \times 4$	$2 \times 2 \times 2$
S2	$4 \times 4 \times 4$	$2 \times 2 \times 2$
2D	4×4	$2 \times 2 (\times 1)$
1D	4	$2 (\times 1 \times 1)$

symmetry was verified using the FINDSYM code.[87]

3 Results and Discussion

In Fig. 3 a visualization of every 3D crystallographic unit cell is provided and in Table 2, the numerical details of the obtained geometries are summarized. The only significant variations in geometry are the in-plane displacements of the different layers with respect to each other. The interlayer spacings and the lattice parameters associated to the individual melon layer vary negligibly. This is also seen when comparing the computational and experimental lattice parameters, independently if one considers B3LYP-D* or PBE-dDsC (see Table S2 in the ESI†).

In Table 3 the energetic results are summarized. Energies discussed here, unless specified otherwise, are in reference to those calculated with the most sophisticated approach used: the B3LYP-dDsC functional.[78] In contrast to the "D*" dispersion correction, "dDsC" depends on the electronic density and has been successfully applied to various branches of chemistry, from homogeneous catalysis[78] to adsorption on metal surfaces.[89] In order to assess the importance of higher-order dispersion effects, we have also tested the MBD dispersion correction.[82] However, MBD is not parametrized for the hybrid functional B3LYP. Therefore, we use the generalized gradient approximation PBE-MBD,[82–84] which has been demonstrated to be accurate for crystal structure predictions.[90–92]

The formation of the H-bonding network upon going from 1D to 2D melon yields ∼95 kJ/mol stabilization per repeat unit (C$_6$N$_9$H$_3$ "tecton"). Stacking 2D melon yields a similar, additional stabilization. The stabilization energies due to stacking are relatively close for all four polymorphs. Nevertheless, the effect of dispersion is crucial for the relative stabilities, whereas the effect of the vibrational energy is almost negligible. Although differences in stability are negligible when using B3LYP-D*, B3LYP-dDsC evidences energetic differences up to ∼ 10 kJ/mol for the different polymorphs. For comparison, Table S1 in the ESI†reports results for several more functionals.

Since the principal application of *g*-CN is as a light absorber in photocatalytic devices, and the primary quality of interest for such light absorbers is the optical gap E$_{g,opt}$ (See Ref. 93 for the definitions used here), the B3LYP optical gaps are provided in the rightmost column of Table 3. As can be seen from Fig. 5d in ref. 3, the conduction band is essentially flat for melon in the d$_H$ and d$_{Ar-Ar}$ directions, due to the compound's molecular character, yielding very slightly lower indirect gaps than direct gaps. The fundamental gap for all 3D structures is hence formally indirect, but within 0.15 eV of the direct one. It is direct for the 2D and 1D

melon structures.

The exciton binding energy was assumed to be 840 meV (see Ref. 3) based on the Wannier-Mott model. This model to evaluate the exciton binding energy for carbonitrides has proven its reliability compared to the more sophisticated, but also more resource consuming, Bethe-Salpeter Equation[4]. This quantity was thus subtracted from the narrowest fundamental gap to obtain the optical band-gap ($E_{g,opt} \equiv (E_{CB}^{min} - E_{VB}^{max}) - E_b$).

The optical gap for the monolayer was equal to 3.2 eV. The obtained 3D optical gaps range from 2.76 eV (Fina) to 3.08 eV (S1), with Lotsch' melon having a similar gap as Fina's (2.83 eV). The S1 structure is predicted by all methods to be the least stable of the 3D structures and the Fina structure seems the most stable following the accurate methods, and hardly distinguishable energetically from the Lotsch and S2 structures for B3LYP-D*. Fina *et al.* suggest that the difference in packing between their structure and the structure found by Lotsch *et al.* could be due to the use of a sealed ampoule. Other subtle differences between their methods, such as synthesis time and temperature, could also lead to different structures.

The above results explain why it proves challenging to determine the crystallographic nature of melon with high certainty. First, the layers can slide with respect to each other, second, several minima are stable and third, the energetic differences between the structures are small. Together, these factors can also be seen as an explanation for the sometimes amorphous nature of melon.

Different polymorphs having similar formation energies is a common situation in crystal structure prediction of organic molecules. Reliably distinguishing polymorphs is challenging even for modern, dispersion corrected DFT approaches.[94] Given the small energetic difference for melon polymorphs obtained here, we stress the importance of combining theory and experiment in the determination of *g*-CN structures.

Researchers focusing on the photocatalytic quality, rather than structural perfection, of melon, could likely find melon that is overall amorphous, but contains crystalline domains like those found in Fina's and Lotsch's structures, possibly even with the "S2-domains" described here. We could expect that a STM image of crystalline domains of carbon nitrides could unveil "Moire" coincidence patterns helping the resolution of the structure as it was done for graphene supported materials.[95]

As for E$_{g,opt}$, our values are in agreement with the established experimental gap of 2.7 eV, especially when considering the limitations of the Wannier-Mott model. Furthermore, trends within a family, are better described by this model than the absolute values, suggesting that the gap of S1 and S2 should be significantly higher than for the Fina polymorph. A "Jelley"-type[96,97] or "J"-aggregation phenomenon such as that seen in fluorescent, aromatic dyes[98] could be the reason for the lowering of the gap in the 3D crystals with respect to the monolayer.[99] Indeed, the "ladder" and "staircase" organizations of the aromatic units - and with that of their dipole moments - observed here are known to lead to this type of photophysics.[100] This insight could be important to synthetic chemists developing new generations of carbon nitrides.

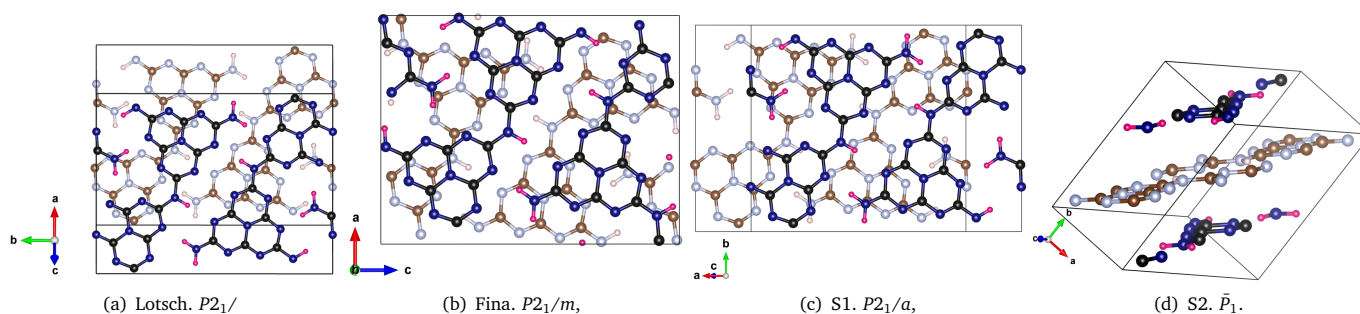| (a) Lotsch. $P2_1/$ | (b) Fina. $P2_1/m$, | (c) S1. $P2_1/a$, | (d) S2. $\bar{P}_1$. |

Fig. 3 Visualization of different crystals in a single unit cell. Black and brown: C; blue shades: N; pink shades: H. The computed unit cells are compared to the experimental ones in Table S2.

Table 2 Tabulation of geometrical results. Distances are reported in Å. Differences with respect to experiment are indicated by a percentage change. Notes: (a) Under "Symmetry" general crystallographic information is listed, *cf.* Fig. 3 and SI. (b) Z is the number of formula units per cell.[88] (c) p2gg is the wallpaper group for this 2D structure. (d) P.O. stands for "pseudo-orthorhombic."

Species	Symmetry[a]	Z[b]	Stacking	d_{Ar-Ar}	d_H	d_{Cov}
1D	Polymer	2	–	–	–	–
2D	p2gg[c]	4	–	–	–	–
Fina	P.O.[d]	8	AB	3.21	+3.12 (+19%)	+1.45 (+11%)
S1	Monoclinic	4	AA	3.24	−3.45 (−21%)	0 (0%)
Lotsch	Monoclinic	4	AA	3.22	0 (0%)	3.43 (+27%)
S2	Primitive	4	AA	3.23	+1.10 (+7%)	−3.35 (−26%)

Table 3 Relative energies (in kJ/mol per tecton; the contribution of the dispersion correction is given in parentheses) and optical gaps (in eV). Notes: (a) $\delta G_{th.}$ is the thermal correction which needs to be added to the electronic energy $\Delta E_{el.}$ in order to obtain the Gibbs free energy ΔG. When comparing the ΔG for the polymorphs, all methods shown here identify Fina as the most stable one. (b) The bandgaps are obtained using the Peintinger-Oliveira-Bredow basis set (cf. Computational Details).

	$\delta G_{th.}$[a] B3LYP-D*	$\Delta E_{el.}$ B3LYP-D*	$\Delta E_{el.}$ PBE-MBD	$\Delta E_{el.}$ B3LYP-dDsC	$E_{g,opt}$ B3LYP[b]
1D	−4	+100 (+8)	+94 (+23)	+97 (+35)	3.05
2D	0	0	0	0	3.22
Fina	+3	−46 (−36)	−68 (−77)	−96 (−116)	2.76
Lotsch	+5	−46 (−37)	−66 (−77)	−88 (−108)	2.83
S1	+5	−44 (−35)	−63 (−81)	−87 (−104)	3.08
S2	+5	−46 (−37)	−65 (−85)	−95 (−114)	3.03
Exp					2.7

4 Conclusions

In summary, we have revisited the polymorphs of melon by density functional theory computations. When taking dispersion interactions accurately into account, our results consistently predict that the Fina polymorph is the most stable, even though other polymorphs are close (within 5 kJ/mol of tectons) in energy. These small energy differences rationalize the experimental observation of different polymorphs depending on the synthesis conditions and suggest that disordered melon structures might be the rule, rather than the exception. The Fina polymorph has also the lowest band-gap ($\sim$ 2.8 eV), in close agreement with experimental estimates. Since it is also the most stable polymorph, we conclude that it most closely represents the commonly produced "melon". However, the S2 polymorph with its 0.2 eV higher band-gap is close in energy, which suggests that it could be accessible via crystal-phase engineering if such a soft-UV band-gap is beneficial for a given application. The bulk band-gap is lowered by 0.2-0.4 eV compared to the 1D and 2D building blocks, indicating that it is a J-type aggregate in the solid state that is responsible for the photoadsorption properties.

Conflicts of interest

There are no conflicts to declare.

Acknowledgements

Acronyms

BSSE basis set superposition error

CN carbon nitride

DFT density functional theory

D3BJ Grimme's D3 formalism with Becke-Johnson damping

MBD many body dispersion

NMR Nuclear Magnetic Resonance

PAW projector augmented-wave

PBE Perdew-Burke-Ernzerhof exchange and correlation functional

VASP Vienna *Ab Initio* Simulation Package

Notes and references

1 N. Lewis and G. Crabtree, *Basic Research Needs for Solar Energy Utilization*, Office of Science US Dept of Energy, 2005.

2 X. Wang, K. Maeda, A. Thomas, K. Takanabe, G. Xin, J. M. Carlsson, K. Domen and M. Antonietti, *Nat. Mater.*, 2009, **8**, 76–80.

3 S. Melissen, T. L. Bahers, S. N. Steinmann and P. Sautet, *J. Phys. Chem. C*, 2015, **119**, 25188–25196.

4 S. N. Steinmann, S. T. A. G. Melissen, T. Le Bahers and P. Sautet, *J. Mater. Chem. A*, 2017, **5**, 5115–5122.

5 M. K. Bhunia, S. T. A. G. Melissen, M. R. Parida, P. Sarawade, J.-M. Basset, D. H. Anjum, O. F. Mohammed, P. Sautet, T. Le Bahers and K. Takanabe, *Chem. Mater.*, 2015, **27**, 8237–8247.

6 X. Li, A. F. Masters and T. Maschmeyer, *ChemCatChem*, 2015, **7**, 121–126.

7 C. Butchosa, P. Guiglion and M. A. Zwijnenburg, *J. Phys. Chem. C*, 2014, **118**, 24833–24842.

8 R. Godin, Y. Wang, M. Zwijnenburg, J. Tang and J. Durrant, *J. Am. Chem. Soc.*, 2017, **139**, 5216–5224.

9 J. McEvoy and G. Brudvig, *Chem. Rev.*, 2006, **106**, 4455–4483.

10 B. A. Pinaud, J. D. Benck, L. C. Seitz, A. J. Forman, Z. Chen, T. G. Deutsch, B. D. James, K. N. Baum, G. N. Baum, S. Ardo, H. Wang, E. Miller and T. F. Jaramillo, *Energy Environ. Sci.*, 2013, **6**, 1983–2002.

11 S. Cao and J. Yu, *J. Phys. Chem. Lett.*, 2014, **5**, 2101–2107.

12 J. Ran, J. Zhang, J. Yu, M. Jaroniec and S. Z. Qiao, *Chem. Soc. Rev.*, 2014, **43**, 7787–7812.

13 F. K. Kessler, Y. Zheng, D. Schwarz, C. Merschjann, W. Schnick, X. Wang and M. J. Bojdys, *Nat. Rev. Mater.*, 2017, **2**, 17030.

14 A. Y. Liu and M. L. Cohen, *Science*, 1989, **245**, 841–842.

15 A. Y. Liu and M. L. Cohen, *Phys. Rev. B*, 1990, **41**, 10727–10734.

16 A. H. Reshak, S. A. Khan and S. Auluck, *RSC Adv.*, 2014, **4**, 6957–6964.

17 J. Gracia and P. Kroll, *J. Mater. Chem.*, 2009, **19**, 3013–3019.

18 S. Zuluaga, L.-H. Liu, N. Shafiq, S. M. Rupich, J.-F. Veyan, Y. J. Chabal and T. Thonhauser, *Phys. Chem. Chem. Phys.*, 2015, **17**, 957–962.

19 Y. Xu and S.-P. Gao, *Int. J. of Hydrog. Energy*, 2012, **37**, 11072–11080.

20 H. Dong, A. R. Oganov, Q. Zhu and G.-R. Qian, *Sci. Rep.*, 2015, **5**, 9870.

21 C. J. Pickard, A. Salamat, M. J. Bojdys, R. J. Needs and P. F. McMillan, *Phys. Rev. B*, 2016, **94**, 094104.

22 S. T. A. G. Melissen, S. N. Steinmann, T. Le Bahers and P. Sautet, *J. Phys. Chem. C*, 2016, **120**, 24542–24550.

23 T. Botari, W. P. Huhn, V. W.-h. Lau, B. V. Lotsch and V. Blum, *Chem. Mater.*, 2017, **29**, 4445–4453.

24 W. Wei and T. Jacob, *Phys. Rev. B*, 2013, **87**, 085202.

25 J. Sehnert, K. Baerwinkel and J. Senker, *J. Phys. Chem. B*, 2007, **111**, 10671–10680.

26 P. Guiglion, C. Butchosa and M. A. Zwijnenburg, *J. Mater. Chem. A*, 2014, **2**, 11996.

27 P. Guiglion, C. Butchosa and M. A. Zwijnenburg, *Macromol. Chem. Phys.*, 2016, **217**, 344–353.

28 V. W.-h. Lau, M. B. Mesch, V. Duppel, V. Blum, J. Senker and B. V. Lotsch, *J. Am. Chem. Soc.*, 2015, **137**, 1064–1072.

29 V. W.-H. Lau, I. Moudrakovski, T. Botari, S. Weinberger, M. B. Mesch, V. Duppel, J. Senker, V. Blum and B. V. Lotsch, *Nat. Commun.*, 2016, **7**, 12165.

30 V. W.-H. Lau, V. W.-Z. Yu, F. Ehrat, T. Botari, I. Moudrakovski, T. Simon, V. Duppel, E. Medina, J. K. Stolarczyk, J. Feldmann, V. Blum and B. V. Lotsch, *Adv. Energy Mater.*, 2017, **7**, 1602251.

31 D. He, C. Zeng, C. Xu, N. Cheng, H. Li, S. Mu and M. Pan, *Langmuir*, 2011, **27**, 5582–5588.

32 H. Cheng, L. Chen, A. C. Cooper, X. Sha and G. P. Pez, *Energy Environ. Sci.*, 2008, **1**, 338–345.

33 S. Tao, L.-J. Yu, R. Pang, Y.-F. Huang, D.-Y. Wu and Z.-Q. Tian, *J. Phys. Chem. C*, 2013, **117**, 18891–18903.

34 X. Li, G. Hartley, A. J. Ward, P. A. Young, A. F. Masters and T. Maschmeyer, *J. Phys. Chem. C*, 2015, **119**, 14938–14946.

35 B. V. Lotsch, M. Döblinger, J. Sehnert, L. Seyfarth, J. Senker, O. Oeckler and W. Schnick, *Chem. – Eur. J.*, 2007, **13**, 4969–80.

36 Y. Zhang, J. Liu, G. Wu and W. Chen, *Nanoscale*, 2012, **4**, 5300–5303.

37 G. Zhang, J. Zhang, M. Zhang and X. Wang, *J. Mater. Chem.*, 2012, **22**, 8083–8091.

38 X. Li, S. T. Melissen, T. Le Bahers, P. Sautet, A. F. Masters, S. N. Steinmann and T. Maschmeyer, *Chem. Mater.*, 2018, **0**, null.

39 A. Schwarzer, T. Saplinova and E. Kroke, *Coord. Chem. Rev.*, 2013, **257**, 2032–2062.

40 F. Fina, S. K. Callear, G. M. Carins and J. T. S. Irvine, *Chem. Mater.*, 2015, **27**, 2612–2618.

41 J. Yi, W. El-Alami, Y. Song, H. Li, P. M. Ajayan and H. Xu, *Chem. Eng. J.*, 2020, **382**, 122812.

42 Y. Hou, A. B. Laursen, J. Zhang, G. Zhang, Y. Zhu, X. Wang, S. Dahl and I. Chorkendorff, *Angew. Chem. Int. Ed.*, 2013, **52**, 3621–3625.

43 S. Arra, R. Babar and M. Kabir, *Phys. Rev. Materials*, 2019, **3**, 095402.

44 H. Chung and Y. Diao, *J. Mater. Chem. C*, 2016, **4**, 3915–3933.

45 Y. Abe, V. Savikhin, J. Yin, A. C. Grimsdale, C. Soci, M. F. Toney and Y. M. Lam, *Chem. Mater.*, 2017, **29**, 7686–7696.

46 S. M. Malathy Sony and M. N. Ponnuswamy, *Cryst. Growth Des.*, 2006, **6**, 736–742.

47 L. Seyfarth, J. Seyfarth, B. V. Lotsch, W. Schnick and J. Senker, *Phys. Chem. Chem. Phys.*, 2010, **12**, 2227–2237.

48 S. L. Mayo, B. D. Olafson and W. A. Goddard, *J. Phys. Chem.*, 1990, **94**, 8897–8909.

49 L. Seyfarth and J. Senker, *Phys. Chem. Chem. Phys.*, 2009, **11**, 3522–3531.

50 J. Liu, H. Wang and M. Antonietti, *Chem. Soc. Rev.*, 2016, **45**, 2308–2326.

51 A. D. Becke, *J. Chem. Phys.*, 1993, **98**, 5648–5652.

52 A. D. Becke, *Phys. Rev. A*, 1988, **38**, 3098–3100.

53 C. Lee, W. Yang and R. G. Parr, *Phys. Rev. B*, 1988, **37**, 785–789.

54 R. Dovesi, R. Orlando, A. Erba, C. M. Zicovich-Wilson, B. Civalleri, S. Casassa, L. Maschio, M. Ferrabone, M. De La Pierre, P. D'Arco, Y. Noël, M. Causà, M. Rérat and B. Kirtman, *Int. J. Quant. Chem.*, 2014, **114**, 1287–1317.

55 R. Dovesi, V. R. Saunders, C. Roetti, R. Orlando, C. M. Zicovich-Wilson, B. Pascale, B. Civalleri, K. Doll, N. M. Harrison, I. J. Bush, P. D'Arco, M. Llunell, M. Causà and Y. Noël, *CRYSTAL14 User's Manual (University of Torino)*, 2014.

56 C. Gatti, V. R. Saunders and C. Roetti, *J. Chem. Phys.*, 1994, **101**, 10686–10696.

57 R. Ditchfield, W. J. Hehre and J. A. Pople, *J. Chem. Phys.*, 1971, **54**, 724–728.

58 M. F. Peintinger, D. V. Oliveira and T. Bredow, *J. Comput. Chem.*, 2013, **34**, 451–459.

59 I. Pelant and J. Valenta, *Luminescence Spectroscopy of Semiconductors*, Oxford University Press: Oxford U.K., 2012.

60 T. Le Bahers, M. Rérat and P. Sautet, *J. Phys. Chem. C*, 2014, **118**, 5997–6008.

61 S. Melissen, F. Labat, P. Sautet and T. Le Bahers, *Phys. Chem. Chem. Phys.*, 2015, **17**, 2199–2209.

62 S. Petit, S. T. A. G. Melissen, L. Duclaux, M. T. Sougrati, T. Le Bahers, P. Sautet, D. Dambournet, O. J. Borkiewicz, C. Laberty-Robert and O. Durupthy, *J. Phys. Chem. C*, 2016, **120**, 24521–24532.

63 T. A. Kandiel, D. H. Anjum, P. Sautet, T. Le Bahers and K. Takanabe, *J. Mater. Chem. A*, 2015, **3**, 8896–8904.

64 T. Le Bahers, S. Haller, T. L. Mercier and P. Barboux, *J. Phys. Chem. C*, 2015, **119**, 17585–17595.

65 A. BaQais, A. Curutchet, A. Ziani, H. Ait Ahsaine, P. Sautet, K. Takanabe and T. Le Bahers, *Chem. Mater.*, 2017, **29**, 8679–8689.

66 A. Ziani, C. Le Paven, L. Le Gendre, F. Marlec, R. Benzerga, F. Tessier, F. Cheviré, M. N. Hedhili, A. T. Garcia-Esparza, S. Melissen, P. Sautet, T. Le Bahers and K. Takanabe, *Chem. Mater.*, 2017, **29**, 3989–3998.

67 B. Civalleri, C. M. Zicovich-Wilson, L. Valenzano and P. Ugliengo, *CrystEngComm*, 2008, **10**, 405–410.

68 D. Presti, A. Pedone, I. Ciofini, F. Labat, M. C. Menziani and C. Adamo, *Theor. Chem. Acc.*, 2016, **135**, 1–11.

69 S. Grimme, *J. Comput. Chem.*, 2006, **27**, 1787–1799.

70 1 Hartree or "Atomic Unit" $\hat{=}$ 27.211 eV $\hat{=}$ 2625.5 kJ $\cdot$ mol^{-1}. 1 atm $\hat{=}$ 1.01325 Pa.

71 G. Kresse and D. Joubert, *Phys. Rev. B*, 1999, **59**, 1758–1775.

72 G. Kresse and J. Hafner, *Phys. Rev. B*, 1993, **47**, 558–561.

73 G. Kresse and J. Hafner, *Phys. Rev. B*, 1994, **49**, 14251–14269.

74 G. Kresse and J. Furthmüller, *Comput. Mater. Sci.*, 1996, **6**, 15–50.

75 G. Kresse and J. Furthmüller, *Phys. Rev. B*, 1996, **54**, 11169–11186.

76 S. F. Boys and F. de Bernardi, *Mol. Phys.*, 1970, **19**, 553–566.

77 P. Jurečka, J. Černý, P. Hobza and D. R. Salahub, *J. Comput. Chem.*, 2007, **28**, 555–569.

78 S. N. Steinmann and C. Corminboeuf, *J. Chem. Theory Comput.*, 2011, **7**, 3567–3577.

79 S. Grimme, S. Ehrlich and L. Goerigk, *J. Comput. Chem.*, 2011, **32**, 1456–1465.

80 J. P. Perdew, K. Burke and M. Ernzerhof, *Phys. Rev. Lett.*, 1996, **77**, 3865–3868.

81 J. P. Perdew, K. Burke and M. Ernzerhof, *Phys. Rev. Lett.*, 1997, **78**, 1396–1396.

82 A. Tkatchenko, R. A. DiStasio, R. Car and M. Scheffler, *Phys. Rev. Lett.*, 2012, **108**, 236402.

83 A. Ambrosetti, A. M. Reilly, R. A. DiStasio and A. Tkatchenko, *J. Chem. Phys.*, 2014, **140**, 18A508.

84 T. Bučko, S. Lebègue, T. Gould and J. G. Ángyán, *J. Phys. Condens. Matter*, 2016, **28**, 045201.

85 H. J. Monkhorst and J. D. Pack, *Phys. Rev. B*, 1976, **13**, 5188–5192.

86 J. Paier, M. Marsman, K. Hummer, G. Kresse, I. C. Gerber and J. G. Ángyán, *J. Chem. Phys.*, 2006, **124**, 154709.

87 H. T. Stokes and D. M. Hatch, *J. Appl. Crystallogr.*, 2005, **38**, 237–238.

88 L. Glasser, *J. Chem. Educ.*, 2011, **88**, 581–585.

89 S. Gautier, S. N. Steinmann, C. Michel, P. Fleurat-Lessard and P. Sautet, *Phys. Chem. Chem. Phys.*, 2015, **17**, 28921–28930.

90 J. G. Brandenburg and S. Grimme, *Acta Crystallogr. Sect. B*, 2016, **72**, 502–513.

91 N. Marom, R. A. DiStasio, V. Atalla, S. Levchenko, A. M. Reilly, J. R. Chelikowsky, L. Leiserowitz and A. Tkatchenko, *Angew. Chem. Int. Ed.*, 2013, **52**, 6629–6632.

92 L. Kronik and A. Tkatchenko, *Acc. Chem. Res.*, 2014, **47**, 3208–3216.

93 J.-L. Bredas, *Mater. Horiz.*, 2014, **1**, 17–19.

94 G. J. O. Beran, *Chem. Rev.*, 2016, **116**, 5567–5613.

95 B. Wang, M.-L. Bocquet, S. Marchini, S. GÃijnther and J. Wintterlin, *Phys. Chem. Chem. Phys.*, 2008, **10**, 3530–3534.

96 E. E. Jelley, *Nature*, 1936, **138**, 1009–1010.

97 E. E. Jelley, *Nature*, 1937, **139**, 631–632.

98 Y.-Y. Liao, S. T. Melissen, J. Audibert, T. Vu, G. Clavier, R. Méallet-Renault, P. Retailleau, J. Lemaistre, V. Génot and R. Pansu, *ChemPhotoChem*, **2**, 72–80.

99 F. C. Spano and C. Silva, *Annu. Rev. Phys. Chem.*, 2014, **65**, 477–500.

100 W. J. Harrison, D. L. Mateer and G. J. T. Tiddy, *J. Phys. Chem.*, 1996, **100**, 2310–2321.